A Queueing Based Scheduling Approach to Plug-In Electric Vehicle Dispatch in Distribution Systems

Qiao Li, *Student Member, IEEE,* Rohit Negi, *Member, IEEE,* and Marija D. Ilić, *Fellow, IEEE*

***Abstract*—Large-scale integration of plug-in electric vehicles (PEV) in power systems can cause severe issues to the existing distribution system, such as branch congestions and significant voltage drops. As a consequence, smart charging strategies are crucial for the secure and reliable operation of the power system. This paper tries to achieve high penetration level of PEVs with the existing distribution system infrastructure by proposing a smart charging algorithm that can optimally utilize the distribution system capacity. Specifically, the paper proposes a max-weight PEV dispatch algorithm to control the PEV charging rates, subject to power system physical limits. The proposed max-weight PEV dispatch algorithm is proved to be throughput optimal under very mild assumptions on the stochastic dynamics in the system. This suggests that the costly distribution system infrastructure upgrade can be avoided, or failing that, at least successfully deferred. The proposed PEV dispatch algorithm is particularly attractive in integrating the renewable energy sources in the distribution system, by successfully absorbing their intermittency.**

***Index Terms*—Plug-in electric vehicle, smart charging, max-weight algorithm, distribution system, renewable energy sources, fluid limits.**

I. Introduction

PLUG-IN electric vehicles (PEV) are widely envisioned to be the key solution to the society's energy security challenges [1], due to its great potential in reducing the whole society's dependence on foreign oil or petroleum, as well as improving the carbon footprint of the transportation sector. As major automakers are planning to produce a diverse range of PEVs in the near future [1], utility companies are becoming increasingly concerned with the adverse impacts of the uncoordinated PEV charging to the power system, in particular at the distribution level [2]. Several studies have shown that [2], [3], the current distribution system, which was planned and built based on historical load demand decades ago, can only accommodate around 10% PEV penetration level in typical scenarios if all PEVs charge in an uncoordinated fashion. As the PEV penetration level increases, the uncoordinated charging can cause severe impacts on the distribution system, such as significant branch congestion and large voltage drops [2], [4]. Thus, in order to achieve large-scale deployment of PEVs in the existing power system, it is crucial to design smart PEV charging strategies, so that not only the PEV energy demands can be successfully satisfied, but also the power system can operate in a secure and reliable manner, without the costly upgrade of the existing infrastructure, or failing that, successfully defer a major upgrade. In other words, the 'physical' structure can be reused or efficiently utilized through intelligent design of the 'cyber' infrastructure in the future cyber-physical electric power system.

In the past research, the coordinated PEV charging has been investigated by many researchers, such as [2], [4], [5], [6]. Despite these interesting research results, there are relatively few research addressing the coordinated PEV charging considering the physical limits in the power system. On the other hand, it is important to notice that such constraints are vital for the reliable operation of the power system, in particular because a PEV will become the biggest energy-consuming device in the household [7], which is very likely to cause severe grid stress if managed inappropriately [2]. A brief summary of the past research papers that consider such physical constraints is as follows. [8] proposes a heuristic method for real-time PEV charging scheduling considering the voltage constraints in the system, where the PEVs are selected in a greedy manner. In [9], a deterministic optimization is adopted to compute the PEV charging schedules, assuming perfect knowledge of non-PEV loads and all PEV driving patterns ahead of time. A real-time PEV charging algorithm is also proposed in [10] for low-voltage distribution systems, where the overall goal is to deliver the maximum amount of total power to the PEV batteries, subject to power system constraints.

As a result of the fundamental power system constraints, the successful integration of PEVs into the existing power system, as well as the capability of utilizing PEVs to provide ancillary vehicle-to-grid services [11], relies crucially on the smart charging algorithm's ability to utilize the 'capacity region' of the existing power system. Informally, such 'capacity region' is defined as the set of feasible PEV loads, subject to the power system constraints, such as branch rating, voltage limits and charging circuit rating. Note that it is highly challenging to utilize the 'capacity region' efficiently, since it can vary significantly over time due to various random factors, such as the non-PEV loads and distributed generation with renewable energy sources. Whereas the later is both time varying and highly intermittent, and therefore is very difficult to predict ahead of time, the former can also be hard to characterize and predict, as it can respond to the time varying electricity price with the implementation of demand response [12].

In this paper, we take a rigorous approach to design smart charging algorithms that can utilize the distribution system 'capacity region' optimally. As a major contribution of this paper, we propose a max-weight PEV dispatch algorithm, based on a queueing formulation of the PEV charging problem.

This work was supported in part by the US NSF under awards CNS-0831973 and ECCS-0931978, and by US ARO award W911NF0710287. All authors are with the Department of Electrical and Computer Engineering, Carnegie Mellon University, Pittsburgh, PA, 15213 USA email:{qiaol, negi, milic}@ece.cmu.edu.

According to the algorithm, the PEV charging rates are computed in real time, based on the current PEV battery states and the other related system parameters, such as non-PEV loads and renewable generation. The PEV dispatch can efficiently coordinate the PEV charging rates subject to power system constraints, and therefore can always guarantee the secure and reliable operation of the power system. More interestingly, the proposed PEV dispatch algorithm is guaranteed to optimally utilize the 'capacity region' of the distribution system, in the sense that the algorithm achieves the optimal throughput asymptotically. Specifically, we develop a theoretic framework, which guarantees the throughput optimality of the proposed PEV dispatch algorithm under very mild assumptions on the stochastic dynamics in the power system. This implies that, intuitively, with such algorithms, the existing power grid can accommodate the highest PEV penetration level without costly upgrade on the existing infrastructure. Further, this algorithm is also very valuable in achieving the vehicle-to-grid services, by providing larger 'capacity margin' for providing ancillary services. Finally, the algorithm is very promising to be implemented with the advent of the widely available information and communication technology (ICT), such as the advanced metering infrastructure (AMI), which enables the distribution system operator (DSO) to efficiently manage the PEV loads in real time.

The rest of the paper is organized as follows. Section II formulates the optimal PEV charging problem, and Section III proposes the max-weight PEV dispatch algorithm. Section IV proves the throughput optimality of the algorithm, and Section V demonstrates the simulations results. Finally, Section VI concludes this paper.

II. Optimal PEV Charging Problem

A. PEV Battery Queueing Model

A discrete-time system is considered in this paper, where the length of each time slot matches the sampling and operation time scale of the DSO, which is on the order of minutes [4], [10]. As the PEV loads are delay tolerant, it is natural to model the battery of each PEV as a queue $U_i(n)$ of 'energy jobs', which has the following dynamics:

$$U_i(n) = [U_i(n-1) - \eta_i \Delta t P_i(n)]^+ + A_i(n), \ \forall i, n \quad (1)$$

In above, the queue length $U_i(n)$ represents the amount of 'energy jobs' that needs to be served by the PEV charger to successfully refill the battery of PEV i. $[\cdot]^+ = \max(\cdot, 0)$, since queue lengths can not be negative. $A_i(n)$ is the amount of external 'energy job' arrivals during time slot n, due to the energy consumption from driving. $P_i(n)$ is the charging power, η_i is the efficiency of the charging circuit, and Δt is the length of the time slot. The charging power $P_i(n)$ is subject to the charging circuit rating constraint:

$$P_i^{\min} \le P_i(n) \le P_i^{\max}, \quad \text{for all PEV } i \quad (2)$$

Further, the charging process is also constrained by the PEV availability, so that

$$P_i(n) = 0 \text{ if } a_i(n) = 0, \quad \text{for all PEV } i \quad (3)$$

where $a_i(n)$ the indicator that PEV i is allowed to draw energy from the power grid during time slot n. This is specified by both the physical availability of PEV i for the charging circuit, i.e., whether PEV i is plugged into the power grid, and the charging control signals by the DSO. In the later case, it is possible that the DSO will curtail the charging processes of certain PEVs, in order to provide vehicle-to-grid services. Note that such 'on-off' assumption is not without loss of generality for vehicle-to-grid services, since the granularity of an individual PEV load is relatively small [7] in terms of providing vehicle-to-grid services. Finally, as the goal of this paper is to achieve the largest capacity region, the PEV availability $a_i(n)$ in this paper is modeled as an external control signal, which is given in each time slot.

B. Charging Constraints

As a PEV is the biggest energy consuming device in a household, it is crucial that not only the PEV batteries can be successfully refilled, but also that the power system can operate in an efficient, reliable and secure manner. In this paper, we model the physical constraint in the distribution system as the voltage limits for each bus:

$$V_k^{\min} \le V_k(n) \le V_k^{\max}, \text{for each bus } k. \quad (4)$$

It is well-known that the PEV charging power can cause significant voltage drop to buses in the power system [2]. This is specified by the network coupling, which is as follows. For each time slot, the impact of the PEV load on the power system states can be described by the AC power flow equations:

$$\begin{aligned} P_k^{\text{net}} + P_k &= V_k \sum_{j \in \mathcal{N}_k} V_j [G_{kj} \cos(\theta_k - \theta_j) + B_{kj} \sin(\theta_k - \theta_j)] \\ Q_k^{\text{net}} &= V_k \sum_{j \in \mathcal{N}_k} V_j [G_{kj} \sin(\theta_k - \theta_j) - B_{kj} \cos(\theta_k - \theta_j)] \end{aligned} \quad (5)$$

where $P_k(n)$ represent the PEV load at bus k, $P_k^{\text{net}}(n)$ and $Q_k^{\text{net}}(n)$ are the net injection of active and reactive power for the non-PEV load:

$$P_k^{\text{net}}(n) = P_k^{\text{base}}(n) - P_k^{\text{renew}}(n) \quad (6)$$

$$Q_k^{\text{net}}(n) = Q_k^{\text{base}}(n) - Q_k^{\text{renew}}(n) \quad (7)$$

where $P_k^{\text{renew}}(n)$ and $Q_k^{\text{renew}}(n)$ are the active and reactive renewable generation for a bus k with distributed generation, and zero otherwise. Thus, if the charging processes of PEVs are uncoordinated, it is well possible that the PEV charging at one bus can make the voltage constraint at a remote bus become violated. On the other hand, if the charging processes of all PEVs are coordinated carefully, it is very promising that not only the power system can operate reliably, but also the highly intermittent renewable energy sources can be successfully 'absorbed' to refill the PEV batteries.

Note that, intuitively, the above constraints (2), (3), (4) and (5) specify a 'capacity region' on the PEV charging rates in each time slot n, which is not only time varying, but also highly stochastic, because of the changes in the base load $P_k^{\text{base}}(n), Q_k^{\text{base}}(n)$, the intermittent renewable generation $P_k^{\text{renew}}(n), Q_k^{\text{renew}}(n)$, as well as the PEV availability $a_i(n)$. It is also important to note that the charging rate can vary

significantly over the locations of the PEVs. For example, the voltage drops at all buses in the power system are much less sensitive to a PEV located close to the substation than a PEV located at the end of the main feeder. Thus, in order to efficiently utilize the capacity region that is available, it is crucial for the DSO to specify the PEV charging rates judiciously, in order to successfully refill all PEV batteries.

III. Max-Weight PEV Dispatch Algorithm

As stated in the Introduction, this paper advocates a max-weight PEV dispatch algorithm for efficient control of the PEV charging rates in each time slot. It will be shown later that the algorithm can optimally utilize the time-average 'capacity region' of the power system asymptotically, even in the presence of the highly intermittent renewable generation.

The real-time PEV dispatch algorithm is illustrated in Algorithm 1. The charging rates are computed by DSO for each time slot, after it collects system-wide information using smart metering infrastructure, such as AMI. The central step is the optimization in (8), which essentially solves an optimal power flow problem, by treating the PEV charging power as *negative* generation. The charging weight (or negative generation cost) for each PEV is specified by $U_i(n)$. Thus, a PEV with larger energy queue length is more likely to draw energy from the power grid, in order to decrease its energy queue length, and vice versa.

Algorithm 1 Max-Weight PEV Dispatch

1: At the beginning of each time slot n, DSO collects $a_i(n)$, $U_i(n)$ for all PEV i, and the non-PEV load profile $P_k^{\text{net}}(n)$ and $Q_k^{\text{net}}(n)$ for all buses.

2: DSO computes charging rates $\{P_i(n)\}$ as follows:

$$\begin{aligned} &\text{maximize}_{\{P_i\}} \sum_{i=1}^{N} U_i(n)\eta_i P_i \\ &\text{subject to} \quad \text{Charging circuit constraint in } (2), \forall \text{PEV } i \\ &\qquad\qquad\ \ \text{PEV availability in } (3), \forall \text{PEV } i \\ &\qquad\qquad\ \ \text{Voltage constraint in } (4), \forall \text{bus } k \\ &\qquad\qquad\ \ \text{AC power flow in } (5), \forall \text{bus } k \end{aligned} \tag{8}$$

3: DSO sends the charging rates $P_i(n)$ to each PEV i.

The PEV dispatch algorithm is easy to implement, as it is executed in real time, based on only current system state information. Note that the optimization in (8) utilizes the energy queue length as the weight for computing charging rates. This is the key to guarantee that the algorithm can achieve throughput optimality over the long term. Other algorithms, in particular the one that maximizes the unweighted charged energy in one time slot, is well known to be sub-optimal in the literature. In this case, the batteries with large energy queue lengths are essentially 'penalized', which may grow very large, as the algorithm always tries to serve PEVs with small queues in the worst case scenario. In the next section, we will develop a theory to formally prove the throughput optimality of Algorithm 1, with very mild assumptions on the stochastic dynamics in the power system.

IV. A Theory on Throughput Optimality

For the ease of demonstration, we first convert the original system to a system with discrete modes. Note that all symbols in bold fonts, such as $\boldsymbol{P}$ and $\boldsymbol{Q}$, represent vectors.

A. An Equivalent Discrete System

The 'capacity region' of the distribution system in each time slot depends crucially on both non-PEV loads and PEV availability at each bus. In order to analyze the performance of the PEV dispatch algorithms in a rigorous manner, we formally denote these external parameters in a compact form as the vector of system 'mode' $\boldsymbol{s} = (\boldsymbol{P}^{\text{net}}, \boldsymbol{Q}^{\text{net}}, \boldsymbol{a})$. It is also assumed that all real power and reactive power in the system are discrete. Note that this is only for the ease of analysis, and is without loss of generality, since the quantization step sizes can be made arbitrarily small. Thus, the system 'mode' vector $\boldsymbol{s}$ take values in a discrete set, which we denote as $\mathcal{S}$. For a fixed discrete system mode $\boldsymbol{s} \in \mathcal{S}$, the PEV charging power vector $\boldsymbol{P}$ are only allowed to take values in a bounded, discrete 'capacity region' $\mathcal{C}(\boldsymbol{s})$, according to the physical limits. This is a discretized region of the feasible region in (8). With the above notations, the PEV battery queueing dynamics can be rewritten in a very compact form as follows:

$$U_i(n) = U_i(0) - \sum_{\boldsymbol{s}} \sum_{\boldsymbol{P}} T_{\boldsymbol{s}}^{\boldsymbol{P}}(n)\eta_i P_i \Delta t + \Lambda_i(n) \tag{9}$$

$$\sum_{\boldsymbol{P}} T_{\boldsymbol{s}}^{\boldsymbol{P}}(n) = T_{\boldsymbol{s}}(n), \tag{10}$$

$$\sum_{\boldsymbol{s}} T_{\boldsymbol{s}}(n) = n, \tag{11}$$

$$T_{\boldsymbol{s}}^{\boldsymbol{P}}(n) \text{ is non-decreasing.} \tag{12}$$

In above, $T_{\boldsymbol{s}}^{\boldsymbol{P}}(n)$ is the total number of time slots that a particular PEV charging rate profile $\boldsymbol{P}$ is chosen when the system mode is $\boldsymbol{s}$ during the first n time slots. Note that $\boldsymbol{P} \in \mathcal{C}(\boldsymbol{s})$, due to physical limits. Thus, (12) follows naturally. The role of DSO is to control the PEV charging rate profiles intelligently, as represented by $T_{\boldsymbol{s}}^{\boldsymbol{P}}(n)$, to make all queue lengths small. $T_{\boldsymbol{s}}(n)$ is the total number of time slots that the system is in mode $\boldsymbol{s}$, according to the definition in (10). Thus, (11) follows naturally, since the system has to be in one mode during each time slot. $\Lambda_i(n)$ represents the cumulative external energy job arrivals to the energy queue of PEV i during the first n time slots.

The system specification in (9)-(12) includes many stochastic processes, such as the net load $\boldsymbol{P}^{\text{net}}, \boldsymbol{Q}^{\text{net}}$, the PEV availability $\boldsymbol{a}$, and the PEV energy job arrivals $\boldsymbol{\Lambda}$. Such processes are driven by very complex external dynamics, such as the intermittent wind power generation, and the PEV driving patterns, which are very challenging to model accurately. Thus, in this paper, instead of specifying restricted assumptions on these stochastic processes, we only the following very mild technical assumptions on these processes, as follows:

Assumption 1: The number of energy job arrivals in each time slot is uniformly bounded:

$$\Lambda_i(n) - \Lambda_i(n-1) \leq K_1, \forall n, i \tag{13}$$

where K_1 is a positive constant.

Assumption 2: The Strong Law of Large Numbers (SLLN) applies to all external stochastic processes in the system:

$$\lim_{n\to\infty} \Lambda_i(n)/n = \lambda_i, \text{ with probability 1,} \forall i \tag{14}$$

$$\lim_{n\to\infty} T_{\boldsymbol{s}}(n)/n = \pi_{\boldsymbol{s}}, \text{ with probability 1,} \forall \boldsymbol{s} \in \mathcal{S} \tag{15}$$

where λ_i is the average energy job arrival rate to the battery of PEV i, and $\pi_{\boldsymbol{s}}$ is the average time fraction that the system mode is at $\boldsymbol{s}$.

Note that such assumptions are very mild, and can be used to model many sources of uncertainties in the power system, in particular the random PEV driving patterns and intermittent renewable generation. Based on the described system model above, we are now able to quantitatively specify the 'throughput region' of the PEV charging in the distribution system, in the following theorem.

Theorem 1: (Throughput Region) The PEV battery queues are rate stable only if there is a static resource allocation policy $\{\mu_{\boldsymbol{s}}^{\boldsymbol{P}}\}$, which satisfies that $\mu_{\boldsymbol{s}}^{\boldsymbol{P}} \geq 0, \sum_{\boldsymbol{P}} \mu_{\boldsymbol{s}}^{\boldsymbol{P}} = \pi_{\boldsymbol{s}}$, and that

$$\lambda_i \leq \sum_{\boldsymbol{s}} \sum_{\boldsymbol{P}} \mu_{\boldsymbol{s}}^{\boldsymbol{P}} \eta_i P_i \Delta t \tag{16}$$

A battery energy queue $U_i(n)$ is defined as 'rate stable' if

$$\lim_{n\to\infty} \frac{U_i(n)}{n} = 0, \text{ with probability 1.} \tag{17}$$

Intuitively, (16) specifies that the average energy job 'arrival rate' at each PEV i can be successfully served by the average energy job 'departure rate' under certain *static policy*, which is specified by the resource allocation decisions $\{\mu_{\boldsymbol{s}}^{\boldsymbol{P}}\}$, where $\mu_{\boldsymbol{s}}^{\boldsymbol{P}}$ specifies the time fraction that PEV charging rate profile $\boldsymbol{P}$ is adopted when the system mode is at $\boldsymbol{s}$. Thus, if the battery energy queues are not rate stable under any resource allocation decisions $\{\mu_{\boldsymbol{s}}^{\boldsymbol{P}}\}$, it is clear that the existing distribution system cannot accommodate the corresponding PEV penetration level, and that an upgrade on the existing infrastructure may be necessary.

Proof: The proof of the theorem is a standard result, and therefore is omitted due to space limit. One can find a standard proof, for example, in [13]. ■

Although the capacity region in Theorem 1 is well defined, it is highly challenging to characterize, even if one has perfect knowledge of the system parameters $\pi_{\boldsymbol{s}}$, due to the large size of the problem. It is even more challenging to design optimal scheduling algorithms to achieve such region. As a major contribution of this paper, we prove that the max-weight PEV dispatch in Algorithm 1 is throughput optimal asymptotically. Before stating the formal proof, we provide intuitive explanation by transforming the original system to a continuous system, where the analysis is much easier. Later we will show that such transformation preserves the optimality guarantee of the algorithm.

B. Fluid Sample Paths

The following continuous-time, deterministic system is referred to as a Fluid Sample Path (FSP) [14] of the original discrete-time, stochastic system:

$$\bar{U}_i(t) = \bar{U}_i(0) - \sum_{\boldsymbol{s}} \sum_{\boldsymbol{P}} \bar{T}_{\boldsymbol{s}}^{\boldsymbol{P}}(t) \eta_i P_i \Delta t + \lambda_i(t) \tag{18}$$

$$\sum_{\boldsymbol{P}} \bar{T}_{\boldsymbol{s}}^{\boldsymbol{P}}(t) = \pi_{\boldsymbol{s}} t \tag{19}$$

$$\bar{T}_{\boldsymbol{s}}^{\boldsymbol{P}}(t) \text{ is non-decreasing.} \tag{20}$$

Note that in order to distinguish between the functions in two systems, a function $f(\cdot)$ in the original system is denoted as $\bar{f}(\cdot)$ in the FSP. It is important to notice the differences between the FSP in (18)-(20) and the discrete system in (9)-(12). In FSP, both energy job arrivals and system modes are deterministic, which can be seen from (18) and (19), respectively, whereas these processes are highly stochastic in the original system. Such deterministic behavior dramatically simplifies the design and analysis of the PEV charging algorithm. Further, such system is rigorously constructed from the original system. The detailed construction is highly nontrivial, and is briefly illustrated in Appendix A. The following theorem shows that the max-weight property in (8) is still preserved in the FSP:

Theorem 2: (Max-Weight Property in FSP) For any FSP associated with the max-weight scheduling, $\dot{\bar{T}}_{\boldsymbol{s}}^{\boldsymbol{P}}(t) = 0$ if

$$\boldsymbol{P} \notin \arg\max_{\boldsymbol{P}'} \sum_{i=1}^{N} \bar{U}_i(t) \eta_i P_i' \tag{21}$$

Thus, for any FSP associated with the max-weight algorithm, the charging mode $\boldsymbol{P}$ always maximizes the fluid energy queue length weighted PEV charging rate.

Proof: See Appendix B. ■

Based on the above theorem, we can now analyze the optimality of the max-weight algorithm in any FSP.

Theorem 3: (Optimality in FSP) For any feasible energy demand rate $\boldsymbol{\lambda}$, any fluid limit under the max-weight charging algorithm satisfies that $\bar{U}_i(t) = 0, \forall t \geq 0$ if $\bar{U}_i(0) = 0, \forall i$.

Proof: For a fixed fluid limit sample path, define the following Lyapunov function

$$L(t) = \frac{1}{2} \sum_{i=1}^{N} (\bar{U}_i(t))^2 \tag{22}$$

It is sufficient to prove that $\dot{L}(t) \leq 0$. We have

$$\begin{aligned}\dot{L}(t) &= \sum_{i=1}^{N} \bar{U}_i(t)\dot{\bar{U}}_i(t) \\ &= \sum_{i=1}^{N} \bar{U}_i(t)\Big(- \sum_{\boldsymbol{s}} \sum_{\boldsymbol{P}} \dot{\bar{T}}_{\boldsymbol{s}}^{\boldsymbol{P}}(t)\eta_i P_i \Delta t + \lambda_i \Big) \\ &\overset{(a)}{\leq} \sum_{i=1}^{N} \bar{U}_i(t)\Big(- \sum_{\boldsymbol{s}} \sum_{\boldsymbol{P}} \dot{\bar{T}}_{\boldsymbol{s}}^{\boldsymbol{P}}(t)\eta_i P_i \Delta t \\ &\qquad + \sum_{\boldsymbol{s}} \sum_{\boldsymbol{P}} \mu_{\boldsymbol{s}}^{\boldsymbol{P}} \eta_i P_i \Delta t \Big) \\ &= - \sum_{\boldsymbol{s}} \sum_{\boldsymbol{P}} \big(\dot{\bar{T}}_{\boldsymbol{s}}^{\boldsymbol{P}} - \mu_{\boldsymbol{s}}^{\boldsymbol{P}}\big)\Big(\sum_{i=1}^{N} \bar{U}_i(t) P_i \eta_i \Delta t \Big) \\ &\overset{(b)}{\leq} 0. \end{aligned} \tag{23}$$

where (a) is because the energy job arrival rate $\boldsymbol{\lambda}$ is feasible, and therefore can be stabilized by a static policy, according to Theorem 1. (b) is because the max-weight property of the Algorithm 1 in FSP, which is guaranteed by Theorem 2. Therefore, the theorem follows. ■

C. Performance Guarantees

With the introduction of the FSP above, we are now ready to prove the main result in this paper, which specifies the throughput optimality of the max-weight PEV dispatch algorithm in Algorithm 1.

Theorem 4: (Optimality in Original System) Under Algorithm 1, for a feasible energy demand rate $\boldsymbol{\lambda}$, all battery energy queues are rate stable with probability 1.

Proof: The proof is in Appendix C. ■

Thus, we have established a theory to guarantee the optimality of the max-weight PEV dispatch algorithm. The performance of the algorithm will next be investigated in the case study in the following section.

V. Case Study

A. Simulation Setup

1) System Loads: The standard IEEE 13-bus test feeder [15] is studied in this paper, which corresponds to a real-world distribution system. The topology of the test feeder is shown in Fig. 1, where the colored (black and gray) nodes represent the buses associated with residential loads. In order to demonstrate the potential of PEVs in integrating intermittent renewable energy sources, it is assumed that a wind generator is installed at bus 671, which is the gray node in Fig. 1. The wind generation pattern for the simulation period is shown in Fig. 2, which is obtained from a real-world data trace in a Pennsylvania wind farm [16]. The simulation considers an over-night charging scenario from 7pm to 5am in the next day. It is assumed that all PEVs are always already plugged-in during the simulation period, and are always available for charging. Thus, $a_i(n) = 1$ for all PEV i and time slot n. The non-PEV residential load profile is specified by the real-world data trace from the SCE website [17]. For each time slot, the load at each bus is obtained by scaling the SCE load profile proportionally according to the case file description [15].

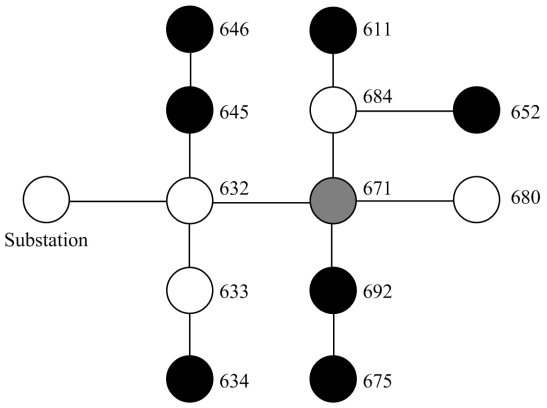

Fig. 1. The topology of the standard IEEE 13-bus test feeder in the case study. The colored nodes are associated with residential loads. A wind generator is placed in the system at bus 671 (the gray node).

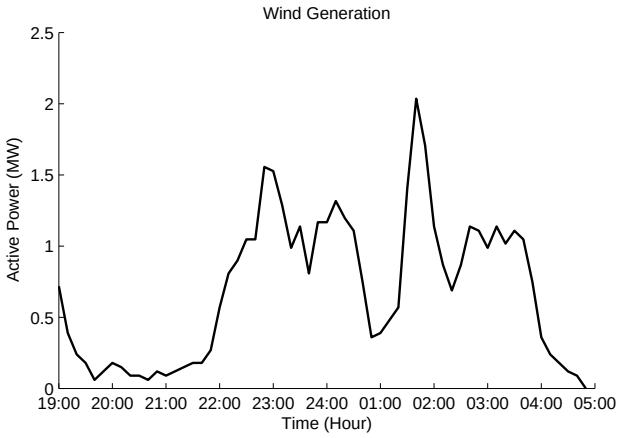

Fig. 2. The wind generation output profile in the case study.

2) PEV Specification: The PEVs are allocated to the buses associated with residential loads, according to Fig. 1. The number of PEVs associated with each bus is proportional to the estimate of the number of households for each bus, which is obtained according to the average daily load specification in the case file of the test feeder. For this simulation, the total number of PEVs in the system is 2185, which corresponds to the 50% penetration scenario. It is assumed that the maximum charging power of each PEV charger is 1.92kW, which corresponds to the standard 120V, 16A charger. For the charging simulation, it is assumed that the energy queue lengths for all PEV batteries are 8.8 kWh. This is according to the national survey of 25 miles average daily commute distance, and the PEV consumption rate of 34 kWh/100 miles [18]. A summary of the PEV specification for this simulation is in Table I.

B. Simulation Results

1) Solution Method: As the PEVs are large loads, it is no longer accurate to model its impact on the power system with conventional linear approximation techniques. For this simulation, the optimal AC power flow in (8) is computed by the technique of sequential convex programming [19],

TABLE I
VEHICLE FACTS

Parameter	Value
Battery Capacity	16 kWh
Energy Usage per 100 miles	34 kWh
Charging Rate (120 V, 16 A)	1.92 kW
Average Daily Commute Distance	25 miles
Daily Consumption	8.75 kWh
Charging Efficiency	0.90

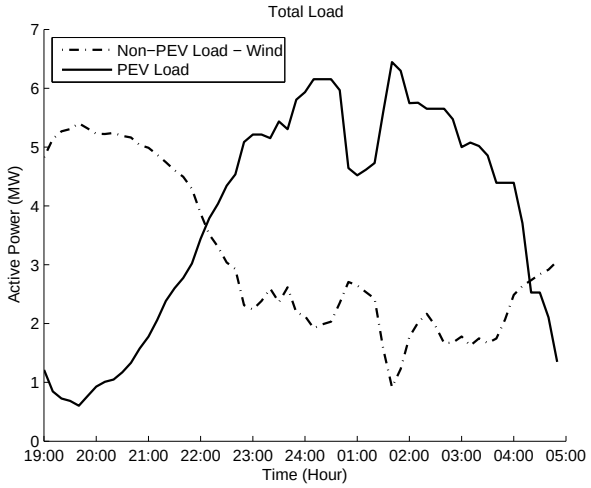

Fig. 3. The load profiles according to the PEV dispatch algorithm.

which works as follows. At each step, the algorithm tries to obtain a local convex approximation of the original nonconvex optimization problem, and then tries to solve the approximated convex problem in a local region and obtain the PEV charging rates. The algorithm then solves the AC power flow with the updated PEV charging rates, and continues to approximate the nonconvex problem (8) at the new operating point, and search for locally optimal solutions. The algorithm will stop if certain convergence criterion is satisfied. For this simulation, the AC power flow is solved using the standard OpenDSS software. The total computation time is around 10^3 seconds on a workstation with 64-bit Windows operating system running with 2.26GHz Intel Duo processor and 8GB RAM.

2) System Load Profiles: The resulting system load profiles are shown in Fig. 3, where the dotted line illustrates the non-PEV load minus the wind generation, and the solid line corresponds to the total PEV load. Note that the dotted load profile is no longer smooth, due to the integration of the highly intermittent wind generation. From the figure, one can clearly observe that the PEV charging is 'smart', in the sense that the total PEV load profile changes very adaptively to both the wind generation and non-PEV load profiles. For example, during the peak hour (around 8pm), when the non-PEV load is very large, the PEV load is quite small, in order to guarantee that the physical limits are not violated and that the power system can operate in a secure and reliable manner. Further, one can easily observe a 'symmetry' between the net load profile and the PEV load profile, in particular during the mid-night, in that an increase in the dotted load profile usually results in a decrease in the PEV load profile, and vice versa. In

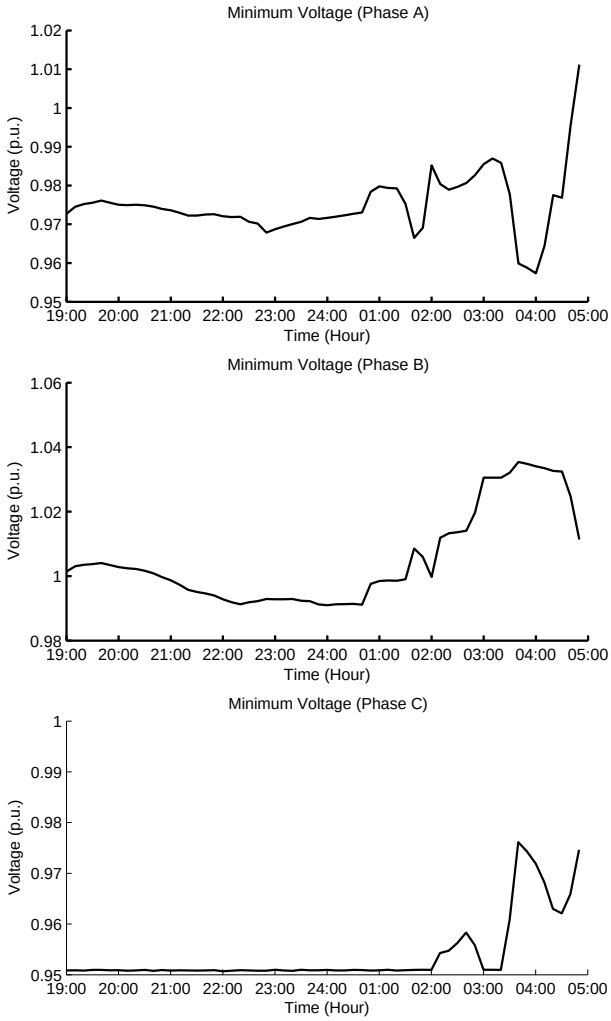

Fig. 4. The profiles of the minimum three phase voltages in the case study.

particular, as the dotted load suddenly drops around 2am, due to the sudden increase in the wind power generation output, one can clearly identify a very similar increase in the total PEV charging profile. This immediately implies that the PEV dispatch algorithm can successfully integrate the renewable wind generation by absorbing its intermittency. Finally, one can observe the sharp decrease in the total PEV load in the morning of the next day. This indicates that most PEVs are successfully refilled.

3) Voltage Profiles: The minimum voltage profiles for each phase in the case study are shown in Fig. 4. One can clearly observe that, the phase C is the bottle neck of the system, as it has the lowest magnitude among all three phases. Note that, interestingly, even if the voltages in the other two phases are far away from the limit (0.95 per unit in this case study), the corresponding PEV loads are still not allowed to charge more, due to the coupling between the phases. Further, note that the minimum voltage in the entire power system is always above the physical limit. Thus, we conclude that the PEV dispatch algorithm in Algorithm 1 can successfully control the charging rates of all PEVs in the power system to maintain reliable operation of the power system. This also partially explains the symmetry between the dotted load profile and the PEV

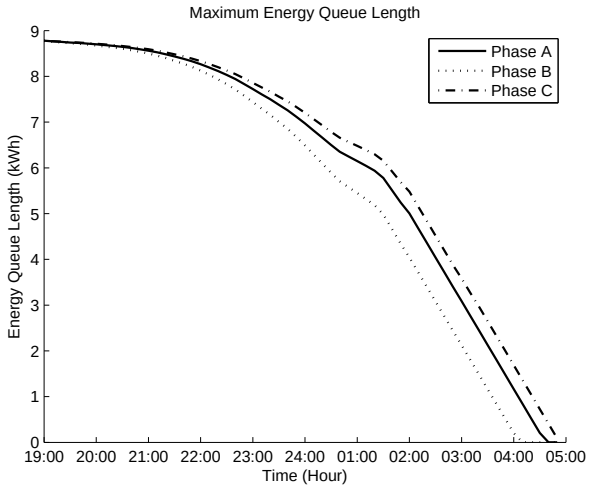

Fig. 5. The profile of the maximum energy queue lengths for each phase in the case study.

load profile in Fig. 3, in that such constraint essentially places an upper bound on the total load in the power system, so that when the net load decreases due to wind power generation, the PEV load will increase, and vice versa. However, it is important to notice that one cannot simply substitute the constraints in (8) with an upper bound on the total system load, since such simplistic method will be very likely to result in excessive voltage drops at certain buses, as suggested in Fig. 4. Finally, one can observe the increase in the minimum voltage near the end of the overnight charging period. This is because many PEVs finish charging.

4) Battery States: In order to demonstrate the performance of the PEV dispatch in refilling the PEV batteries, we plot the profiles of the maximum energy queue lengths for each phase in Fig. 5. The conclusion is that, for all three phases, the PEV dispatch algorithm can successfully refill all PEV batteries during the overnight charging period. Further, the figure also confirms the coupling of the charging processes between the three phases, which is suggested in Fig. 4, in that even if the voltage limit in the phase A and B are far from the boundary, the PEV loads are not allowed to charge further during the charging period, due to their coupling effect to the voltage in phase C, which is the bottleneck of the network. Thus, the maximum energy queue lengths in all three phases behave very similarly, with the PEV loads in phase B finish relatively earlier, due to the fact that it is the least constrained in voltage, according to Fig. 4. Similarly, the PEV loads in phase A also finish earlier than phase C. Further, a more careful inspection reveals that at the beginning of the charging period, the charging rate is relatively low, in order to avoid the power system congestion. The charging rate becomes much higher near the end of the charging period. This is because, during such period, the charging processes are essentially only constrained by the rating of the PEV charging circuits.

VI. Conclusion

This paper proposes a queueing based scheduling approach to achieve large-scale integration of PEVs into the existing power system. Based on the queueing formation, a max-weight PEV dispatch algorithm is formulated, and is proved to be throughput optimal, under very mild assumptions on the stochastic dynamics of the power system. Simulation results demonstrate that, the proposed PEV dispatch algorithm can not only successfully integrate the PEVs into the existing power system, but also absorb the highly intermittent wind power generation, as well as guarantee the secure and reliable operation of the power system.

Appendix A
Construction of Fluid Limits

Given the network dynamics $(\boldsymbol{U}(n), \boldsymbol{\Lambda}(n), T_{\boldsymbol{s}}^{\boldsymbol{P}}(n))_{n=0}^{\infty}$, we first extend the support from $\mathbb{N}$ to $\mathbb{R}_+$ using linear interpolation. For a fixed sample path ω, define the following fluid scaling:

$$f^r(t,\omega) = f(rt,\omega)/r, \tag{24}$$

where the function $f(\cdot)$ can be $U_i(\cdot), \Lambda_i(\cdot)$ or $T_{\boldsymbol{s}}^{\boldsymbol{P}}(\cdot)$. It can be verified that these functions are uniformly Lipschitz-continuous, i.e., there is a positive constant $K_2 > 0$ such that

$$|f^r(t+\delta) - f^r(t)| \quad \leq \quad K_2\delta \tag{25}$$

for any r, $t > 0$ and $\delta > 0$. Thus, these functions are equi-continuous. According to the Arzéla-Ascoli Theorem [20], any sequence of functions $\{f^{r_n}(t)\}_{n=1}^{\infty}$ contains a subsequence $\{f^{r_{n_k}}(t)\}_{k=1}^{\infty}$, such that w.p.1,

$$\lim_{k\to\infty} \sup_{\tau\in[0,t]} |f^{r_{n_k}}(\tau) - \bar{f}(\tau)| = 0 \tag{26}$$

where $\bar{f}(t)$ is a uniformly continuous function, and therefore differentiable almost everywhere [20]. Define any such limit $(\bar{\boldsymbol{U}}(t), \bar{\boldsymbol{\Lambda}}(t), \bar{T}_{\boldsymbol{s}}^{\boldsymbol{P}}(t))$ as a fluid limit.

Now, the equations in (18) and (19) follow naturally from the discrete-time system by taking $k \to \infty$ along a convergent subsequence. The deterministic energy job arrival processes and the deterministic system mode processes in (19) are because of the SLLN, by assumption.

Appendix B
Proof of Theorem 2

Proof: According to (21), there is another feasible schedule $\boldsymbol{P}' \in \mathcal{C}(\boldsymbol{s})$, so that

$$\sum_{i=1}^{N} \bar{U}_i(t) P_i \eta_i \leq \sum_{i=1}^{N} \bar{U}_i(t) P_i' \eta_i + \varepsilon \tag{27}$$

for some constant $\varepsilon > 0$. Since all functions in FSP are uniformly continuous, there is $\delta > 0$, such that for any $\tau \in (t-\delta, t+\delta)$, we have

$$\sum_{i=1}^{N} \bar{U}_i(\tau) P_i \eta_i \leq \sum_{i=1}^{N} \bar{U}_i(\tau) P_i' \eta_i + \frac{\varepsilon}{2} \tag{28}$$

Now, since all scaled functions $f^{r_{n_k}}(t)$ converge to the fluid limits uniformly on compact set along the subsequence $\{n_k\}$, there is a constant K, such that for any $k > K$, we have

$$\sum_{i=1}^{N} U_i^{r_k}(\tau) P_i \eta_i \leq \sum_{i=1}^{N} U_i^{r_k}(\tau) P_i' \eta_i + \frac{\varepsilon}{4} \tag{29}$$

for any $\tau \in (t-\delta, t+\delta)$ in the scaled system. Recall the definition of fluid scaling, the above implies that

$$\sum_{i=1}^{N} U_i(\tau) P_i \eta_i \leq \sum_{i=1}^{N} U_i(\tau) P_i' \eta_i + \frac{r_{n_k}\varepsilon}{4} \tag{30}$$

for any $\tau \in (r_{n_k}(t-\delta), r_{n_k}(t+\delta))$ in the original unscaled system. According to Algorithm 1, the PEV charging rate profile $\boldsymbol{P}$ is never scheduled during $\tau \in (r_{n_k}(t-\delta), r_{n_k}(t+\delta))$, which implies that $T_{\boldsymbol{s}}^{\boldsymbol{P}}(r_{n_k}\tau)$ is a constant for any $\tau \in (t-\delta, t+\delta)$ and $k > K$. Thus, after taking $k \to \infty$, we conclude that $\bar{T}_{\boldsymbol{s}}^{\boldsymbol{P}}(\tau)$ is also constant during $(t-\delta, t+\delta)$, from which the theorem follows. ■

APPENDIX C
PROOF OF THEOREM 4

Proof: Assume that the claim does not hold. Then, according to the definition of rate stability, there is a subsequence $\{r_k\}$ and some i, such that

$$\lim_{k\to\infty} U_i(r_k)/r_k \geq \varepsilon \tag{31}$$

for some $\varepsilon > 0$. Now, according to Appendix A, we can obtain a subsequence $\{r_{n_k}\}$ which converges to a FSP. Note that in this case, we have

$$\bar{U}_i(1) \geq \varepsilon, \tag{32}$$

which contradicts Theorem 3. Therefore, the network is rate stable and the theorem holds. ■

REFERENCES

[1] A. Boulanger, A. Chu, S. Maxx, and D. Waltz, "Vehicle electrification: Status and issues," *Proc. IEEE*, vol. 99, no. 6, pp. 1116–1138, Jun. 2011.

[2] J. Lopes, F. Soares, and P. Almeida, "Integration of electric vehicles in the electric power system," *Proc. IEEE*, vol. 99, no. 1, pp. 168–183, Jan. 2011.

[3] K. Schneider, C. Gerkensmeyer, M. Kintner-Meyer, and R. Fletcher, "Impact assessment of plug-in hybrid vehicles on pacific northwest distribution systems," in *Proc. Power Energy Soc. Gen. Meet.*, Jul. 2008, pp. 1–6.

[4] K. Clement-Nyns, E. Haesen, and J. Driesen, "The impact of charging plug-in hybrid electric vehicles on a residential distribution grid," *IEEE Trans. Power Syst.*, vol. 25, no. 1, pp. 371–380, Feb. 2010.

[5] E. Sortomme, M. Hindi, S. MacPherson, and S. Venkata, "Coordinated charging of plug-in hybrid electric vehicles to minimize distribution system losses," *IEEE Trans. Smart Grid*, vol. 2, no. 1, pp. 198–205, Mar. 2011.

[6] D. Wu, D. Aliprantis, and K. Gkritza, "Electric energy and power consumption by light-duty plug-in electric vehicles," *IEEE Trans. Power Syst.*, vol. 26, no. 2, pp. 738–746, May 2011.

[7] A. Brooks, E. Lu, D. Reicher, C. Spirakis, and B. Weihl, "Demand dispatch," *IEEE Power and Energy Magazine*, vol. 8, no. 3, pp. 20–29, May-Jun. 2010.

[8] S. Deilami, A. Masoum, P. Moses, and M. Masoum, "Real-time coordination of plug-in electric vehicle charging in smart grids to minimize power losses and improve voltage profile," *IEEE Trans. Smart Grid*, vol. 2, no. 3, pp. 456–467, Sep. 2011.

[9] O. Sundstrom and C. Binding, "Flexible charging optimization for electric vehicles considering distribution grid constraints," *IEEE Trans. Smart Grid*, vol. 3, no. 1, pp. 26–37, Mar. 2012.

[10] P. Richardson, D. Flynn, and A. Keane, "Optimal charging of electric vehicles in low-voltage distribution systems," *IEEE Trans. Power Syst.*, vol. 27, no. 1, pp. 268 –279, Feb. 2012.

[11] S. Han, S. Han, and K. Sezaki, "Development of an optimal vehicle-to-grid aggregator for frequency regulation," *IEEE Trans. Smart Grid*, vol. 1, no. 1, pp. 65–72, Jun. 2010.

[12] H. Saele and O. Grande, "Demand response from household customers: Experiences from a pilot study in Norway," *IEEE Trans. Smart Grid*, vol. 2, no. 1, pp. 102–109, Mar. 2011.

[13] L. Tassiulas and A. Ephremides, "Stability properties of constrained queueing systems and scheduling policies for maximum throughput in multihop radio networks," *IEEE Trans. Autom. Control*, vol. 37, no. 12, pp. 1936–1948, Dec. 1992.

[14] J. G. Dai and W. Lin, "Maximum pressure policies in stochastic processing networks," *Oper. Res.*, vol. 53, no. 2, pp. 197–218, Mar. 2005.

[15] W. Kersting, "Radial distribution test feeders," in *Proc. IEEE Power Eng. Soc. Win. Meet.*, vol. 2, 2001, pp. 908–912.

[16] National Renewable Energy Labratory. (2006) Wind integration data sets. [Online]. Available: http://www.nrel.gov/wind/integrationdatasets/eastern/data.html

[17] Southern California Edision. (2011) Regulatory information - SCE load profiles. [Online]. Available: http://www.sce.com/AboutSCE/Regulatory/loadprofiles

[18] P. Hu and T. Reuscher. (2004, Dec.) Summary of travel trends. U.S. Department of Transportation and Federal Highway Administration. [Online]. Available: http://nhts.ornl.gov/2001/pub/STT.pdf

[19] C. Zillober, K. Schittkowski, and K. Moritzen, "Very large scale optimization by sequential convex programming," *Optimization Methods and Software*, vol. 19, no. 1, pp. 103–120, 2004.

[20] H. Royden, *Real Analysis*. Prentice Hall, 1988.

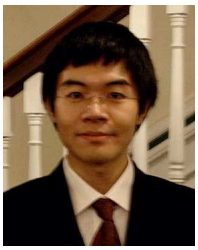

Qiao Li (S'07) received the B.Engg. degree from the Department of Electronics Information Engineering, Tsinghua University, Beijing China, in 2006. He received the M.S. degree from the Department of Electrical and Computer Engineering, Carnegie Mellon University, Pittsburgh, PA USA, in 2008.

He is currently a Ph.D. Candidate in the Department of Electrical and Computer Engineering, Carnegie Mellon University. His research interests include distributed algorithms, smart grid technologies, and wireless networking.

Rohit Negi (S'98-M'00) received the B.Tech. degree in electrical engineering from the Indian Institute of Technology, Bombay, in 1995. He received the M.S. and Ph.D. degrees from Stanford University, CA, in 1996 and 2000, respectively, both in electrical engineering.

Since 2000, he has been with the Electrical and Computer Engineering Department, Carnegie Mellon University, Pittsburgh, PA, where he is a Professor. His research interests include signal processing, coding for communications systems, information theory, networking, cross-layer optimization, and sensor networks. Dr. Negi received the President of India Gold Medal in 1995.

Marija Ilić (M’80-SM’86-F’99) is currently a Professor at Carnegie Mellon University, Pittsburgh, PA, with a joint appointment in the Electrical and Computer Engineering and Engineering and Public Policy Departments. She is also the Honorary Chaired Professor for Control of Future Electricity Network Operations at Delft University of Technology in Delft, The Netherlands. She was an assistant professor at Cornell University, Ithaca, NY, and tenured Associate Professor at the University of Illinois at Urbana-Champaign. She was then a Senior Research Scientist in Department of Electrical Engineering and Computer Science, Massachusetts Institute of Technology, Cambridge, from 1987 to 2002. She has 30 years of experience in teaching and research in the area of electrical power system modeling and control. Her main interest is in the systems aspects of operations, planning, and economics of the electric power industry. She has co-authored several books in her field of interest. Prof. Ilic is an IEEE Distinguished Lecturer.